

# A Theoretical Model of Erosion and Macromolecular Drug Release from Biodegrading Microspheres

RICHARD P. BATYCKY\*, JUSTIN HANES<sup>†</sup>, ROBERT LANGER<sup>‡</sup>, AND DAVID A. EDWARDS<sup>§x</sup>

Received September 27, 1996, from the \*Department of Chemical and Materials Engineering, University of Alberta, Edmonton, Alberta, Canada T6G 2G6, <sup>†</sup>Department of Chemical Engineering, Massachusetts Institute of Technology, Cambridge, MA 02139, and <sup>§</sup>Department of Chemical Engineering, 204 Fenske Lab, Penn State University, University Park, PA 16802. Final revised manuscript received April 24, 1997. Accepted for publication August 24, 1997.<sup>®</sup>

**Abstract** □ A theoretical model is outlined for predicting the time evolution of total mass, mean molecular weight, and drug release for the case of a spherical bulk-eroding microsphere, prepared by a double emulsification procedure and containing a hydrophilic drug, such as a protein or peptide. Explicit analytical formulae are derived for calculating the time evolution of measurable macroscopic characteristics, such as drug release or mean molecular weight. Microsphere hydration, polymer erosion, and drug release phases are each described. Results indicate that polymer degradation by only random-chain scission or only end scission (or unzipping) cannot explain experimentally observed kinetics of particle mass loss and molecular weight change; thus, a combined model (incorporating both random and end scission) is proposed. A general methodology for determining the microscopic transport coefficients (such as polymer degradation rate constant or drug diffusion coefficient) from erosion and release data is outlined. This paradigm is applied to the specific case of 50:50 poly(D,L-lactic-co-glycolic acid (PLGA) microspheres encapsulating glycoprotein 120 (gp 120), a candidate AIDS vaccine. Predictions permit comparisons with experimental data for mean weight- and number-averaged molecular weights, as well as for mass loss and protein release. Other comparisons are made with data appearing in the literature for release of tetanus toxoid from PLA and PLGA microspheres of variable molecular weight. Agreement between theory and experiment is observed.

## Introduction

Current theoretical understanding of drug release from polymeric systems primarily concerns the circumstance of a therapeutic molecule that is insoluble in water, but soluble in the polymer or copolymer phase.<sup>1-3</sup> Attention has largely been restricted to nondegradable devices with macroscopically simple geometries. Increasing interest in the encapsulation and controlled release of macromolecular, "water-soluble" or "polymer-insoluble" therapeutics from degradable polymeric devices makes this case of polymer erosion and drug release as compelling as the water-insoluble therapeutic case, and in some ways more challenging. From the theoretical point of view, complications arise with macromolecular drugs, such as peptides or proteins, because the release of the water-soluble substance is intimately related to the "microporous" (i.e., angstrom- or nanometer-dimension) structure of the copolymer, which for hydrolytically degradable polymers obviously evolves over time in an aqueous environment. Although some success has been made in the past toward understanding the role of pore geometry on effective diffusion rates,<sup>4</sup> no previous approach has succeeded in relating the evolving pore structure of an eroding polymer particle to the concomitant evolving transport properties of released species and, thereby, to overall erosion and drug release rates. A

major obstacle is the sheer complexity of the underlying, highly coupled, mass transport processes involved. In practice, investigators tend to deduce from polymer mass, mean molecular weight, and percent drug release<sup>4-7</sup> important "underlying" data regarding hydration kinetics, polymer degradation mechanisms, and drug diffusion phenomena.<sup>5,6</sup>

In this article, we outline a theoretical framework that permits the prediction of (bulk-eroding) polymer erosion and macromolecular drug release as functions of time and various geometrical, physical, and chemical properties of the polymeric drug delivery system. An explicit microstructural model (based on the hypothesis of coalescing micropores and spatially evolving mesopores) is used to develop general expressions for the following: (1) the rate of polymer mass loss; (2) the rate of mean (mass- and number-average) molecular weight change; and (3) the rate of macromolecular drug release. We test this model by comparison with experimental data and show how it may be used to extract important quantitative information previously known only qualitatively. A paradigm is provided for systematic interpretation of erosion and release data. We use this paradigm to analyze experimental data<sup>8</sup> obtained for the special case of 50:50 poly(D,L-lactic-co-glycolic acid) (PLGA) copolymeric microspheres encapsulating glycoprotein 120 (gp120, a subunit protein currently under investigation as a prophylactic vaccine for HIV-1). Other comparisons with experimental data appearing in the literature are also made. Applications of the theory to more general and complex systems than those to which attention is herein focused are discussed.

## Description of the Erosion and Release Process

Consider the case of a PLGA microsphere (of radius  $r_0$ ) made by a double emulsification procedure<sup>8</sup> to encapsulate a hydrophilic substance, such as a protein or peptide drug. The hydrophilic drug is initially localized primarily in the vicinity of discrete, spherical (or nearly spherical) occlusions (or "macropores"), formed within the microparticle during the particle preparation process and remaining following the removal of water during the drying process. Depending on the method of formation, the microparticle may contain a very large number of extremely small occlusions, or a smaller number of relatively large occlusions. Thus, the terminology "macropores" (versus the micro- and mesopores subsequently discussed) need not be literal. The volume of occlusions is denoted  $V_0$ , and the volume fraction  $\phi_0 = V_0/(\frac{4}{3}\pi r_0^3)$  is less than unity ( $\phi_0 < 1$ ). An illustration of the spherical-occlusion structure of a single microsphere of the type under consideration is shown in Figure 1.

Upon immersing the microsphere within an aqueous buffer, water penetrates toward the center of the microsphere. This penetration occurs with great speed relative to the ultimate time of polymer erosion. For example, water diffuses through a glassy polymer<sup>9</sup> with  $T_g = 40$  °C (case of PLGA) with

<sup>®</sup> Abstract published in *Advance ACS Abstracts*, October 15, 1997.

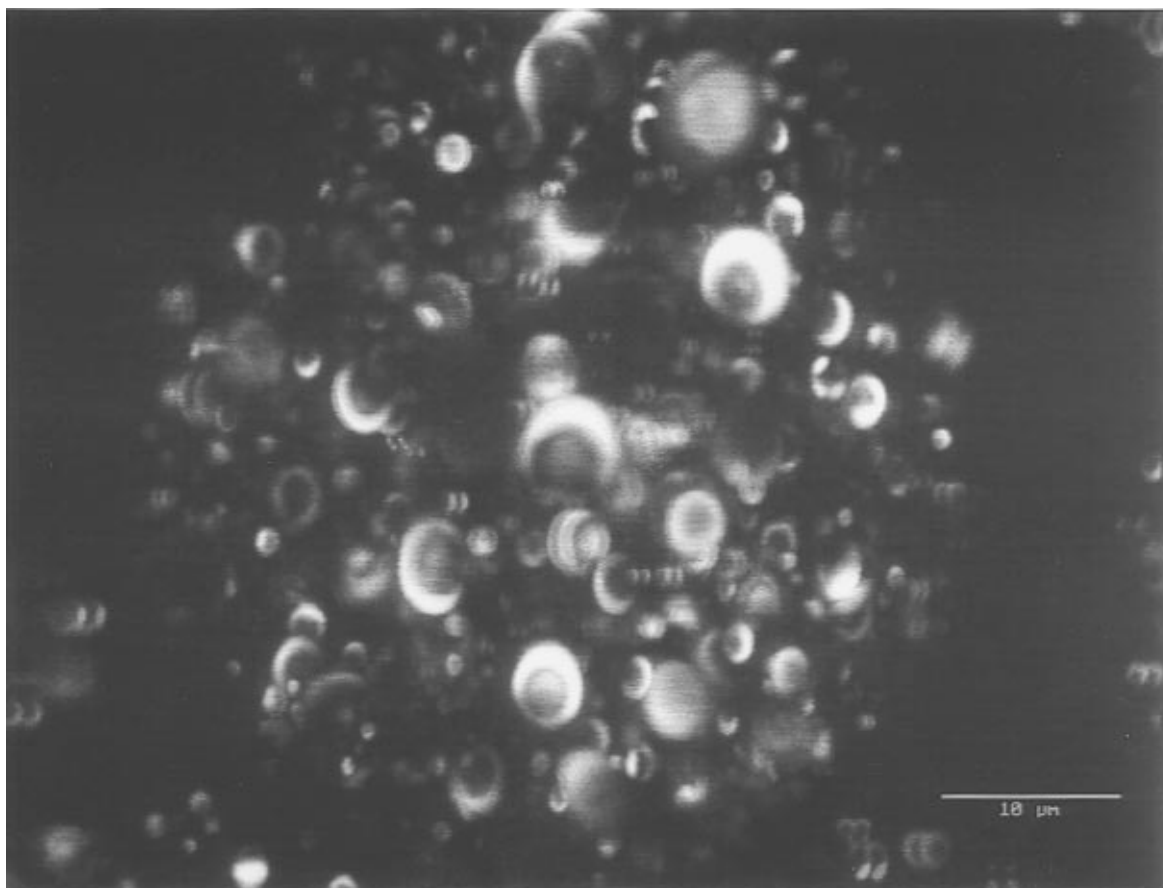


**Figure 1**—Three-dimensional confocal microscopy image depicting the spherical-occlusion structure of a single PLGA microsphere and localization of (fluorescently labeled) drug along the periphery of the occlusions.

diffusivity  $\approx 5 \times 10^{-8} \text{ cm}^2 \text{ s}^{-1}$ ; hence, the characteristic time required for penetration of water molecules to the core of a  $50\text{-}\mu\text{m}$  radius microsphere is  $\approx (50 \mu\text{m})^2 / (5 \times 10^{-8} \text{ cm}^2 \text{ s}^{-1})$  or  $\approx 8 \text{ min}$ .

At the conclusion of this very brief hydration phase, degradation of PLGA copolymers is occurring throughout the microparticle volume. In this “erosion” phase, the micropores grow in size and coalesce because of polymer erosion and oligomer solubilization, forming “mesopores” (see Figure 2) with mean characteristic radial dimension  $RM \gg a_i$ , where  $a_i$  are the Stokes-Einstein radii of released monomers and oligomers. In this phase, the erosion (and ultimate release of hydrophilic macromolecular drug) is necessarily controlled *not* by diffusion through the mesopores, but by the rate of appearance of monomers and oligomers into the mesopores via diffusion through the surrounding microporated matrix; that is, the process is degradation rate controlled. Lastly, it bears noting that the precise ratio of micro- to mesoporous zones within the microsphere will depend intimately on the extent of crystallinity (and therefore LA:GA ratio), polymer molecular weight, and especially microsphere processing parameters.

The relatively large size of the macromolecular drug, at least barring a highly porated polymer structure, prevents release of the substance until the mesoscopic pores reach sufficiently high numbers. Thus, an “induction phase” may occur for protein release when initial porosity is low, as commented upon elsewhere.<sup>4,10</sup> Although the primary macromolecular release will generally occur following the induction phase, protein adsorbed to the surface of the microparticle and within preexisting mesopores may give rise to an initial

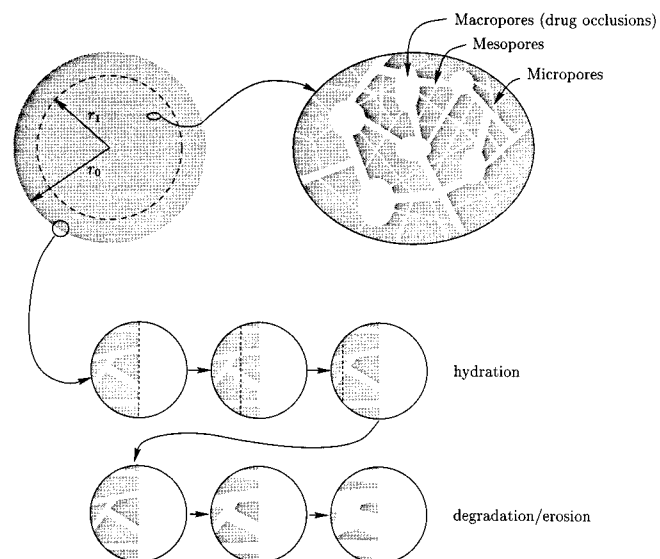


**Figure 2**—A microsphere of radius  $r_0$  undergoing hydration, degradation, and erosion. The latter involves the bulk erosion of the polymeric microsphere (expansion of the pore walls) and, hence, an increase in the porosity  $\epsilon$ .

“burst” of macromolecule release that is controlled by the rate of macromolecule desorption.

It is also possible that some degradation or irreversible aggregation of macromolecular drug may occur because of contact with organic solvent during microsphere preparation, polymer-drug interactions, local acidity due to polymer degradation products, and other reactions.<sup>10</sup>

## Model Equations

An internally consistent model of the foregoing views the molecular-size pores or 'free volume' regions, into which water initially diffuses and from which predegraded solubilized oligomers are released, as circular cylindrical micropores of radius  $R_\mu$ .<sup>11</sup> Assuming these pores to be randomly distributed throughout the particle, the total number ( $N_\mu$ ) of such pores leading from the external particle surface can be related to the microparticle porosity ( $\epsilon$ ; fractional volume containing no polymer) by

$$\epsilon = \epsilon_\mu + \epsilon_M + \phi_0 \quad (1)$$

where

$$\epsilon_\mu = N_\mu \frac{\pi R_\mu^2}{4\pi I_0^2} \quad (2)$$

is the fractional pore space of the micropores and

$$\epsilon_M = N_M \frac{\pi R_M^2}{4\pi I_0^2} \quad (3)$$

is the pore space of mesopores. The three pore populations may be measured by non-mercury porosimetry,<sup>8</sup> as later discussed.

**Assumptions of the Analysis**—In addition to the assumption of micro-, meso-, and macroporous structures already discussed, we assume the following:

(1) The microsphere possesses an outer radius  $r_0$  and a porosity  $\epsilon$ . This porosity includes both mesopores  $\epsilon_M$  and occlusions  $\phi_0$  (such that  $\epsilon = \epsilon_M + \phi_0$  at  $t = 0$ ) each with drug adsorbed to their respective surfaces. The occlusions are entirely embedded within microporated polymer matrix; that is, drug cannot escape from  $\phi_0$  without diffusing through micropores or mesopores that have been formed by coalescence of micropores.

(2) During hydration and erosion, the radius  $r_0$  remains fixed, although the porosity changes with time (see Figure 2).

(3) Water and monomers (and potentially low oligomers; the terminology "monomers" is used in what follows) are able to diffuse through the polymer matrix (i.e., through micropores), yet the macromolecular drug, by virtue of its size and hydrophilicity, is not able to diffuse through the polymer matrix.

(4) The meso- and micropores are assumed to be cylindrical, with radii  $R_M$  and  $R_\mu$ , respectively.

(5) The porosities  $\epsilon_\mu$  and  $\epsilon_M$  and the radii  $R_\mu$  and  $R_M$  are spatially uniform (though variable in time); hence, the number of pores present at any given particle radius varies; namely,

$$N_\mu = \frac{4r^2 \epsilon_\mu}{R_\mu^2} \quad (4)$$

$$N_M = \frac{4r^2 \epsilon_M}{R_M^2} \quad (5)$$

where  $N_\mu$  and  $N_M$  are the numbers of micro- and mesopores, respectively, at sphere radius  $r$ .

(6) The hydration phase occurs instantaneously relative to the erosion phase. Water "tunnels" toward the center of the particle. Degraded low molecular weight oligomers (specifically, in the case of PLGA, this will include monomers to nonamers) diffuse out of the hydrated matrix at rates that are fast compared with polymer degradation rates.

(7) During particle erosion the radii of micropores [ $R_\mu = R_\mu(t)$ ] and mesopores [ $R_M = R_M(t)$ ] change with time.

(8) The drug desorbs from the exterior surface of the microparticle and the surfaces of the mesopores. Desorption is characterized by an initial surface concentration [ $C_d^s(0)$ ] of drug and a rate of desorption ( $k_d$ ); no other interactions between polymer and drug are accounted for, apart from steric interactions that slow down the rate of drug diffusion through the polymer matrix. Release from the occlusions  $\phi_0$  within the microparticle is precluded until the mean pore radius  $\bar{R}$  (leading from the occlusions inside the particle, to the external bath) exceeds the characteristic molecular radius of the drug ( $a_d$ ).

(9) After the induction phase, drug is released from the microsphere in a Fickian manner, characterized by an effective drug diffusivity ( $\bar{D}^*$ ).

(10) A pseudo-steady-state assumption is used, requiring that the rate of change in  $R_\mu$  or  $R_M$  be small compared with diffusion over the length scale of the microsphere:

$$Pe_R = \frac{|dR/dt|r_0}{\bar{D}^*} \ll 1 \quad \forall (R \in \{R_\mu, R_M\}, \bar{D}^* \in \{\bar{D}_d^*, \bar{D}_j^*\}) \quad (6)$$

Degradation and erosion end when the porosity of the sphere approaches unity ( $\epsilon \rightarrow 1$ ) or  $\epsilon_\mu + \epsilon_M \rightarrow 1 - \phi_0$ .

Based on these assumptions, a kinetic degradation model is next proposed, and expressions for the particle mass and mass- and number-averaged mean molecular weights are derived. Models for the desorption, induction, and Fickian release of drug are also developed.

**Microparticle Degradation and Erosion**—To understand particle mass loss and drug release it is first necessary to characterize the nature of the degradation process. We consider a polymer composed of monomers  $j$ , which appear in the ratio  $j_1 : j_2 : \dots : j_J$ , where  $J$  is the number of different monomers. Each monomer is present with the following mole fraction:

$$\phi_j = \frac{j_j}{\sum_{k=1}^J j_k} \quad (7)$$

If the entire polymer were allowed to degrade entirely to monomers, then the "apparent" molecular weight of any one of these monomers (i.e., a monomer chosen at random) would on average have a molecular weight ( $M_1^{\text{bulk}}$ ) defined as follows:

$$M_1^{\text{bulk}} \stackrel{\text{def}}{=} \sum_{i=1}^J \phi_i M_i \quad (8)$$

where  $M_i$  is the molecular weight of the  $i$ th monomer. In the subsequent analysis we need only concern ourselves with *this* apparent molecular weight and not those of different monomers.

The bulk polymer is composed of different amounts of polymer chains of various lengths, with  $n_i(t)$  as the number of moles of polymer chains that are  $i$  monomers in length. The corresponding molecular weight will be (on average)  $M_i^{\text{bulk}}$ . If the monomers combine without mass loss, then one expects  $M_i^{\text{bulk}} = iM_1^{\text{bulk}}$ . If, as in the case of PLGA, there is water addition as a result of chain scission, then one expects the following:

$$M_i^{\text{bulk}} = iM_1^{\text{bulk}} - (i-1)M_{\text{H}_2\text{O}} \quad (9)$$

Now, let  $n_i(t)$  be the number of moles of polymer chains of length  $i$  that are present in the microparticle at time  $t$ . Subsequently, we will develop a model for predicting  $n_i(t)$  given an underlying mechanism, such as random chain scission or end scission.

There are two important ways of viewing the makeup of the polymer particles and, hence, the way in which particle mass and mean molecular weights are calculated; the first involves using the entire distribution, and the second assumes the smallest  $N$  oligomers are "invisible" to the measurement process. In the case of PLGA, where oligomers up to and including nonamers are soluble,<sup>12,13</sup> properties measured with techniques such as gel-phase chromatography (GPC) do not contain contributions from these first nine oligomers ( $N = 9$ ), either because they are not present (they are small enough to have diffused out of the system) or they are present but not measurable. A simple yet instructive example of this is provided by the case of polymer mass. From the definitions of  $n_i(t)$  and  $M_i^{\text{bulk}}$ , the total mass of the polymer  $m_p(t)$  comprising the microsphere at any time  $t$  is given by the following:

$$m_p(t) = \sum_{i=1}^{\infty} M_i^{\text{bulk}} n_i(t) \quad (10)$$

If, however, in the process of measurement the soluble (low) oligomers are removed (e.g., in the case of PLGA,  $N = 9$ ), then the actual measured mass [ $m_p^{\text{part}}(t)$ ] is given by

$$m_p^{\text{part}}(t) = \sum_{i=1+N}^{\infty} M_i^{\text{bulk}} n_i(t) \quad (11)$$

and the "mass gain" caused by water hydration (cf. eq 9) is naturally not detected. Similar arguments can be made for the weight fraction of the  $i$ th chain

$$w_i(t) = \frac{M_i^{\text{bulk}} n_i(t)}{m_p(t)} \quad (12)$$

whose actual measured weight fraction is

$$w_i^{\text{part}}(t) = \begin{cases} \frac{M_i^{\text{bulk}} n_i(t)}{m_p^{\text{part}}(t)}, & \forall (i \geq N + 1) \\ 0, & \forall (1 \leq i \leq N) \end{cases} \quad (13)$$

Also, the mass-averaged mean molecular weight is

$$\bar{M}_w(t) = \frac{1}{m_p(t)} \sum_{i=1}^{\infty} (M_i^{\text{bulk}})^2 n_i(t) \quad (14)$$

with the following actual measured value:

$$\bar{M}_w^{\text{part}}(t) = \frac{1}{m_p^{\text{part}}(t)} \sum_{i=1+N}^{\infty} (M_i^{\text{bulk}})^2 n_i(t) \quad (15)$$

Finally, we note the following definition of number-averaged mean molecular weight:

$$\bar{M}_n(t) = m_p(t) \left[ \sum_{i=1}^{\infty} n_i(t) \right]^{-1} \quad (16)$$

The actual measured value of eq 16 is

$$\bar{M}_n^{\text{part}}(t) = m_p^{\text{part}}(t) \left[ \sum_{i=1+N}^{\infty} n_i(t) \right]^{-1} \quad (17)$$

The preceding formulae can be used to predict the mass and molecular weights of the microsphere by the following model of  $n_i(t)$ .

*General Equations Governing  $n_i(t)$* —The degradation of polymers has been studied extensively, both in terms of statistical arguments<sup>14,15</sup> and kinetic equations<sup>16–21</sup> for discrete and continuous systems. As we are considering a discrete system, the time-dependent amount [ $n_i(t)$ ] of  $i$ -mers ( $i = 1, 2, 3, \dots$ ) within a microsphere undergoing degradation satisfies the following discrete kinetic equation<sup>17</sup>:

$$\frac{dn_i}{dt} = -n_i(t) \sum_{j=1}^{i-1} F_{j,i-j} + 2 \sum_{j=i+1}^{\infty} \frac{F_{i,j}}{j} n_j(t) \quad \forall (1 \leq i) \quad (18)$$

where  $F_{i,j}$  is the intrinsic rate that an  $(i + j)$ -mer breaks up into an  $i$ -mer and a  $j$ -mer. These kinetic equations describe the following general reactions:

$$n_{i+j} \xrightarrow{F_{i,j}} n_i + n_j \quad \forall (1 \leq i, 1 \leq j) \quad (19)$$

These coupled, linear, ordinary differential equations are solved subject to the initial conditions of  $n_i(t) = n_i(0)$  at  $t = 0$ . These equations form the foundation of any degradation model, with each characterized by a different form of  $F_{i,j}$ .

*Random Chain Scission*—Consider the case of "random scission"; that is, where all bonds break with equal probability. For this case, the intrinsic rate is given by:

$$F_{i,j} = k_n \quad (20)$$

where  $k_n$  is the chain scission rate constant, which is independent of time and oligomer length. Equation 18 becomes:

$$\frac{dn_i}{dt} = -(i-1)k_n n_i(t) + 2k_n \sum_{j=i+1}^{\infty} n_j(t) \quad \forall (1 \leq i) \quad (21)$$

which has the following general solution<sup>17</sup>:

$$n_i(t) = e^{-(i-1)k_n t} \{ n_i(0) + \sum_{j=1}^{\infty} n_{i+j}(0) [1 + j - 2j e^{-k_n t} + (j-1)e^{-2k_n t}] \} \quad \forall (1 \leq i) \quad (22)$$

where  $n_i(0)$  is the initial amount of polymer chains of length  $i$ . As  $t \rightarrow \infty$ , we obtain the expected result,  $n_i(t) \rightarrow 0$  for  $i \geq 2$  and the following:

$$n_1(t) |_{t \rightarrow \infty} \rightarrow \sum_{j=1}^{\infty} j n_j(0) \quad (23)$$

*End Scission*—Because of the increased acidity near the ends of each chain, the degradation rate constant near the ends may be larger than the rate constant inward from the ends. To investigate this mechanism, consider the limiting case of "end scission" that is, where only the bonds that produce a monomer and another oligomer break. Furthermore, all chains have an equal probability of undergoing end scission. The intrinsic rate constant for this case is given by:

$$F_{i,j} = \begin{cases} k_n^1 & \forall (i = 1 \text{ or } j = 1) \\ 0, & \forall (i \neq 1 \text{ and } j \neq 1) \end{cases} \quad (24)$$

where  $k_n^1$  is the end scission rate constant, which is independent of time and oligomer length. With this form of  $F_{i,j}$ , eq 18 becomes:

$$\frac{dn_i}{dt} = -2k_n^1 n_i(t) + 2k_n^1 n_{i+1}(t) \quad \forall (3 \leq i) \quad (25)$$

$$\frac{dn_2}{dt} = -k_n^1 n_2(t) + 2k_n^1 n_3(t) \quad (26)$$

$$\frac{dn_1}{dt} = 2k_n^1 \sum_{j=2}^{\infty} n_j(t) \quad (27)$$

This set of coupled, linear, ordinary differential equations must be solved subject to the initial condition  $n_i(t) = n_i(0)$  at  $t = 0$ . The most straightforward way to derive a solution is to realize that in any real system there is a maximum chain length, say  $M$ . Now, because chains are undergoing only scission, the equations are coupled such that  $n_i$  depends on  $n_{i+1}(0)$ ,  $n_{i+2}(0)$ , etc., but not on smaller chain lengths. This dependence means one can solve explicitly for  $n_M(t)$  [in terms of  $n_M(0)$ ], then for  $n_{M-1}(t)$  [in terms of  $n_{M-1}(0)$  and  $n_M(0)$ ], and so on. This procedure produces a pattern in the solution, independent of  $M$ . The general solution is:

$$n_i(t) = e^{-2k_n^1 t} \sum_{j=0}^{\infty} \frac{(2k_n^1 t)^j}{j!} n_{i+j}(0) \quad \forall (3 \leq i) \quad (28)$$

$$n_2(t) = e^{-k_n^1 t} [n_2(0) + \sum_{j=0}^{\infty} 2^{j+1} n_{j+3}(0) P(j+1, k_n^1 t)] \quad (29)$$

where  $P(l, x)$  is the incomplete gamma function,<sup>22</sup> which, for positive integer values of  $l$ , has the following form:

$$P(l, x) = 1 - e^{-x} \sum_{m=0}^{l-1} \frac{x^m}{m!} \quad (30)$$

The solutions of eqs 28 and 29 can then be substituted into the differential equation for  $n_1(t)$ , which then can be solved. A simpler approach is possible by noting that the total number of monomers is conserved; hence, the quantity  $\sum_{i=1}^{\infty} i n_i(t)$  is conserved for all time. The amount of monomers in the microsphere determined by the simpler approach is then given by:

$$n_1(t) = n_1(0) + \sum_{i=2}^{\infty} i [n_i(0) - n_i(t)] \quad (31)$$

Once  $n_2(t)$ ,  $n_3(t)$ , etc., are known from eqs 28 and 29,  $n_1(t)$  can be calculated. Also note that eqs 28 and 29 decay to zero as  $t \rightarrow \infty$ ; hence, the expected limit (eq 23) is obtained.

**Combined Mechanism**—As will be shown later by comparison with experimental data, neither of the two previous mechanisms can account for the observed mass and molecular weight evolutions. Hence, consider now the case of *simultaneous* random chain scission and end scission. The generalized degradation rate is given by:

$$F_{i,j} = \begin{cases} k_n^1 & \forall (i = 1 \text{ or } j = 1), \\ k_n & \forall (i \neq 1 \text{ and } j \neq 1), \end{cases} \quad (32)$$

For this two-rate model, it is useful to introduce a dimensionless time defined in terms of the end scission rate:

$$\tau \stackrel{\text{def}}{=} k_n^1 t \quad (33)$$

and the ratio of the two rates:

$$\gamma \stackrel{\text{def}}{=} \frac{k_n}{k_n^1} \quad (34)$$

where  $\gamma = 1$  corresponds to pure random chain scission and  $\gamma = 0$  to pure end scission. In this context, the governing differential equations become:

$$\frac{dn_i}{d\tau} = -[2 + \gamma(i-3)]n_i(\tau) + 2n_{i+1}(\tau) + 2\gamma \sum_{j=i+2}^{\infty} n_j(\tau) \quad \forall (3 \leq i) \quad (35)$$

$$\frac{dn_2}{d\tau} = -n_2(\tau) + 2n_3(\tau) + 2\gamma \sum_{j=4}^{\infty} n_j(\tau) \quad (36)$$

$$\frac{dn_1}{d\tau} = 2 \sum_{j=2}^{\infty} n_j(\tau) \quad (37)$$

These equations are subject to the initial condition  $n_i(\tau) = n_i(0)$  at  $\tau = 0$ . These coupled, linear, ordinary differential equations may be solved (as in the case of end scission in the previous section) by assuming a maximum chain size  $M$  and successively solving for  $n_M(\tau)$ ,  $n_{M-1}(\tau)$ , etc., to obtain a general solution that is independent of  $M$ . The general form of  $n_i(\tau)$  for  $i \geq 3$  is

$$n_i(\tau) = \sum_{j=0}^{\infty} n_{i+j}(0) \sum_{l=0}^j \frac{B_{j,l}}{\gamma^l} e^{-[2+\gamma(i-3+l)]\tau} \quad \forall (3 \leq i) \quad (38)$$

where the first few values of  $B_{j,l}$  are defined as  $B_{0,0} = 1$ ,  $B_{1,1} = -2$ ,  $B_{2,2} = 2 - \gamma^2$ ,  $B_{1,0} = 2$ ,  $B_{2,1} = -4$ , and  $B_{2,0} = 2 + \gamma^2$ . The remaining values are defined recursively as  $B_{j,l} = 2/l[\{\gamma/2(l-1) - 1\}B_{j-1,l-1} + (\gamma - \gamma^2)B_{j-2,l-2}]$  [ $\forall (3 \leq l \leq j)$ ], and:

$$\left. \begin{aligned} B_{j,2} &= -B_{j-1,1} - \gamma^2 B_{j-2,0} \\ B_{j,1} &= -2B_{j-1,0} \\ B_{j,0} &= -\sum_{l=1}^j B_{j,l} \end{aligned} \right\} \quad \forall (3 \leq j)$$

This solution can then be used in eq 36 to obtain an expression for  $n_2(\tau)$ ; namely,

$$n_2(\tau) = n_2(0)e^{-\tau} + 2 \sum_{j=0}^{\infty} n_{3+j}(0) \sum_{l=0}^j \frac{B_{j,l} e^{-\tau} (1 - e^{-[1+\gamma l]\tau})}{\gamma^l [1 + \gamma l]} + 2\gamma \sum_{m=4}^{\infty} \sum_{j=0}^{\infty} n_{m+j}(0) \sum_{l=0}^j \frac{B_{j,l} e^{-\tau} (1 - e^{-[1+\gamma l(m-3+l)]\tau})}{\gamma^l [1 + \gamma(m-3+l)]} \quad (39)$$

Finally, as a result of conservation of monomers comprising the chains, the result in eq 31 still holds:

$$n_1(\tau) = n_1(0) + \sum_{i=2}^{\infty} i [n_i(0) - n_i(\tau)] \quad (40)$$

The actual implementation of this model is somewhat difficult because of the slow convergence of the summations for small values of  $\gamma$  (i.e., when end scission and random

scission act on very different time scales). Furthermore, as a result of this variation in scales, a numerical discretization of eqs 35 and 36 using an explicit method is quite unstable (unless computationally intensive, small time steps are used); that is, an explicit method must take time steps that are small enough to resolve the end scission process but still numerous enough to resolve the random scission process. Where analytical and explicit numerical techniques fail, however, an *implicit* numerical method excels as a result of the *linearity* and *triangular* nature of the differential equations. The triangular nature of the problem is akin to the way in which the analytical solutions were derived; that is, by solving for the evolution of a maximum chain length  $n_M(\tau)$ , then  $n_{M-1}(\tau)$ , etc., while recognizing that  $n_L(0) = 0$  and hence  $n_L(\tau) = 0$  for all  $L > M$  and all time  $\tau$ .

To implement this implicit method, consider calculating the distribution at a time  $\tau + \Delta\tau$  in terms of the distribution at  $\tau$ . Writing eqs 35 and 36 in a discretized implicit form [with  $n_i^\tau$  and  $n_i^{\tau+\Delta\tau}$  the numerical approximations to  $n_i(\tau)$  and  $n_i(\tau + \Delta\tau)$ , respectively] gives the following:

$$n_M^{\tau+\Delta\tau} = \frac{n_M^\tau}{1 + \Delta\tau[2 + \gamma(M - 3)]} \quad (41)$$

$$n_{M-1}^{\tau+\Delta\tau} = \frac{n_{M-1}^\tau + 2\Delta\tau n_M^{\tau+\Delta\tau}}{1 + \Delta\tau[2 + \gamma(M - 4)]} \quad (42)$$

$$n_i^{\tau+\Delta\tau} = \frac{n_i^\tau + 2\Delta\tau[n_{i+1}^{\tau+\Delta\tau} + \gamma \sum_{j=i+2}^M n_j^{\tau+\Delta\tau}]}{1 + \Delta\tau[2 + \gamma(i - 3)]} \quad \forall (3 \leq i \leq M - 2) \quad (43)$$

$$n_2^{\tau+\Delta\tau} = \frac{n_2^\tau + 2\Delta\tau[n_3^{\tau+\Delta\tau} + \gamma \sum_{j=4}^M n_j^{\tau+\Delta\tau}]}{1 + \Delta\tau} \quad (44)$$

which can be seen to be stable for *any* choice of step size  $\Delta\tau$  regardless of the choice of  $\gamma$ . The convergence properties of this method, as opposed to the stability, will be addressed later. The triangular nature of this problem is made apparent by the fact that eqs 41–44 can be solved in order without the difficult task of inverting a matrix at each time step.<sup>23</sup> The monomer amount is then given by eq 40 as follows:

$$n_1(\tau + \Delta\tau) = n_1(0) + \sum_{i=2}^{\infty} i[n_i(0) - n_i(\tau + \Delta\tau)] \quad (45)$$

A final useful transformation is to cast eqs 41–45 in terms of the following quantity:

$$\hat{w}_i(\tau) \stackrel{\text{def}}{=} \frac{M_i^{\text{bulk}} n_i(\tau)}{m_p(0)} \quad (46)$$

This quantity may be thought of as the weight fraction of chain  $i$  in the absence of a mass increase due to water addition; but, suffice it to say that the practical utility of this quantity stems from the ultimate removal of the mass of the particle [ $m_p(0)$ ] from the calculation of mass and molecular weight change, and hence an independence of results to the size of the sample. The relevant interpretations of eqs 10–17 in the context of  $\hat{w}_i(\tau)$  are given in Table 1. Note that  $\hat{w}_1(0) = w_1(0)$ , meaning that only knowledge of the initial weight fraction distribution (e.g., as obtained by GPC) is needed to compute the relevant quantities.

**Table 1—Formulae for Predicting Particle Mass and Molecular Weight Predictions following Choice of a Degradation Model Describing  $n_i(\tau)$ , or, More Importantly,  $\hat{w}_i(\tau)$**

| Physical  | Actual or Measured   |
|---|--|
| $\frac{m_p(\tau)}{m_p(0)} = \sum_{i=1}^M \hat{w}_i(\tau)$   | $\frac{m_p^{\text{part}}(\tau)}{m_p(0)} = \sum_{i=1+N}^M \hat{w}_i(\tau)$  |
| $w_i(\tau) = \frac{\hat{w}_i(\tau)}{m_p(\tau)/m_p(0)}$  | $w_i^{\text{part}}(\tau) = \begin{cases} \frac{\hat{w}_i(\tau)}{m_p^{\text{part}}(\tau)/m_p(0)} & \forall (i \geq N+1) \\ 0 & \forall (1 \leq i \leq N) \end{cases}$ |
| $\bar{M}_w(\tau) = \frac{\sum_{i=1}^M M_i^{\text{bulk}} \hat{w}_i(\tau)}{m_p(\tau)/m_p(0)}$                       | $\bar{M}_w^{\text{part}}(\tau) = \frac{\sum_{i=1+N}^M M_i^{\text{bulk}} \hat{w}_i(\tau)}{m_p^{\text{part}}(\tau)/m_p(0)}$  |
| $\bar{M}_n(\tau) = \frac{m_p(\tau)}{m_p(0)} \left[ \sum_{i=1}^M \hat{w}_i(\tau) / M_i^{\text{bulk}} \right]^{-1}$ | $\bar{M}_n^{\text{part}}(\tau) = \frac{m_p^{\text{part}}(\tau)}{m_p(0)} \left[ \sum_{i=1+N}^M \hat{w}_i(\tau) / M_i^{\text{bulk}} \right]^{-1}$                      |

Any of these models may now be used in evaluating particle mass or molecular weights (Table 1) once the initial weight distribution, embodied in  $w_i(0)$ , and the rate constant(s)  $k_n$  and/or  $k_n^l$  are chosen.

**Drug Release**—As the microsphere degrades, drug is released by desorption and diffusion. As noted at the outset, desorption is assumed to originate with drug initially contained on the sphere surface and in mesopores connected to the external surface of the microsphere, whereas drug diffusion is delayed by an induction time sufficient to allow for micropores to coalesce and permit the passage of the macromolecular drug out from the occlusions through the micropore matrix.

**Initial Burst**—The radii of mesopores are much larger than that of the drug, so the change in the surface concentration of drug can be modeled as follows:

$$\frac{dC_d^s}{dt} = -k_d C_d^s \quad (47)$$

Equation 47 has the following solution:

$$C_d^s(t) = C_d^s(0) e^{-k_d t} \quad (48)$$

where  $C_d^s(0)$  is the initial surface concentration. The mass of drug remaining in the microsphere during this desorption process is then described as follows:

$$m_d(t) = m_d(0) - M_d A [C_d^s(0) - C_d^s(t)] \quad (49)$$

where  $A$  is the area of the particle undergoing this desorption process. This area is, explicitly,

$$A = 4\pi r_0^2 [1 - \epsilon_\mu - \epsilon_M] + \int_0^{r_0} N_M 2\pi R_M dr \quad (50)$$

upon noting that the occlusions  $\phi_0$  do not penetrate the surface of the sphere. Substituting the definition of  $N_M$  (eq 5) and using the fact that desorption occurs only from surfaces initially exposed [ $\epsilon_\mu = \epsilon_\mu(0)$ ,  $\epsilon_M = \epsilon_M(0)$ ,  $R_M = R_M(0)$ ] yields the following result:

$$A = 4\pi r_0^2 \left[ 1 - \epsilon_\mu(0) - \epsilon_M(0) + \frac{2}{3} \epsilon_M(0) \frac{r_0}{R_M(0)} \right] \quad (51)$$

where it is obvious that the major contribution to  $A$  is the area of the mesopores. The final form of the drug mass expression is then:

$$\frac{m_d(t)}{m_d(0)} = 1 - \phi_d^{\text{burst}}(1 - e^{-k_d t}) \quad (52)$$

where  $\phi_d^{\text{burst}}$  is the mass fraction of drug involved in the burst (adsorbed to the surface of mesopores and outer microsphere surface) relative to the drug initially present, and is defined as follows:

$$\phi_d^{\text{burst}} \stackrel{\text{def}}{=} 4\pi r_0^2 \left[ 1 - \epsilon_\mu(0) - \epsilon_M(0) + \frac{2}{3} \epsilon_M(0) \frac{r_0}{R_M(0)} \right] \frac{M_d c_d^s(0)}{m_d(0)} \quad (53)$$

**Induction Time**—During particle hydration and degradation, the mean volume-averaged pore radius at time  $t$  is

$$\bar{R}(t) = \frac{\epsilon_\mu R_\mu + [\epsilon_M - \epsilon_M(0)] R_M}{\epsilon_\mu + \epsilon_M - \epsilon_M(0)} \quad (54)$$

This mean radius evolves in a complicated fashion that depends on the time evolution of  $\epsilon_\mu$ ,  $\epsilon_M$ ,  $R_\mu$ , and  $R_M$ . We first note that the (measurable) mass of the particle at any time  $t$  is related to the porosities  $\epsilon_\mu$  and  $\epsilon_M$  by the following expression:

$$\frac{m_p^{\text{part}}(t)}{m_p^{\text{part}}(0)} = \frac{1 - \phi_0 - \epsilon_M(t) - \epsilon_\mu(t)}{1 - \phi_0 - \epsilon_M(0) - \epsilon_\mu(0)} \quad (55)$$

This expression shows that the sum  $\epsilon_M(t) + \epsilon_\mu(t)$  appearing in the denominator of eq 54 is known as a function of time once the particle mass loss profile is known. Substituting eq 55 into eq 54, and noting that  $R_M \gg R_\mu$  gives eq 56:

$$\bar{R}(t) \approx \frac{R_M(t) [\epsilon_M(t) - \epsilon_M(0)]}{1 - \phi_0 - \frac{m_p^{\text{part}}(t)}{m_p^{\text{part}}(0)} [1 - \phi_0 - \epsilon_M(0) - \epsilon_\mu(0)]} \quad (56)$$

Hence, the growth of the mean pore radius  $\bar{R}(t)$  can be directly attributed to the growth in the mesopore radius  $R_M(t)$  and/or the growth in the fraction of mesopore space  $\epsilon_M(t)$ . This mean pore growth may be due both to mass loss by polymer degradation and pore coalescence (i.e., micropores coalescing to form mesopores). For example, using eqs 4 and 5 with eq 55, it is possible to show the following:

$$\begin{aligned} \frac{d}{dt}(\epsilon_M + \epsilon_\mu) &= \frac{1}{4r_0^2} \frac{d}{dt} (N_M R_M^2 + N_\mu R_\mu^2) \\ &= \frac{1}{m_p^{\text{part}}(0)} \frac{dm_p^{\text{part}}}{dt} [1 - \phi_0 - \epsilon_M(0) - \epsilon_\mu(0)] \quad (57) \end{aligned}$$

For typical bulk-eroding polymeric systems,  $dm_p^{\text{part}}/dt \approx 0$  for several days following the outset of hydration/degradation (see next section). Nevertheless, mesopores on the surface of the microsphere begin to grow in number from “day 1;”<sup>8</sup> therefore,

from eq 57, in this early time phase

$$\frac{d\epsilon_M}{dt} \approx - \frac{d\epsilon_\mu}{dt} \quad (58)$$

That is, the growth of mesopore space in the early stages of degradation is largely attributable to the loss of microporous space [i.e., by the joining (or coalescing) of micropores to form mesopores]. Specifically, it is found<sup>8</sup> that  $\epsilon_M(t)$  [or, in fact,  $N_M(r_0, t)$ ] grows linearly with time for the first 15 days of degradation of PLGA microspheres, with  $R_M \approx R_M(0)$  approximately constant. In this case, we postulate eq 59 for times sufficiently shorter than the total degradation time:

$$\begin{aligned} \frac{d\epsilon_M}{dt} &= \frac{R_M(0)^2}{4r_0^2} \left. \frac{dN_M}{dt} \right|_{r=r_0} \\ &= \text{const.} \quad (59) \end{aligned}$$

Equation 59 is more explicitly written as follows:

$$\left. \frac{dN_M}{dt} \right|_{r=r_0} = k_{\text{coal}} \quad (60)$$

where  $k_{\text{coal}}$  is a pore coalescence rate (units of reciprocal time). Substituting into eq 56 then yields the following working equation:

$$\bar{R}(t) = \frac{R_M(0)^3 k_{\text{coal}} t}{4r_0^2 [\epsilon_M(0) + \epsilon_\mu(0)]} \quad (61)$$

The drug induction time  $t^d$  is defined here by

$$\bar{R}(t = t^d) = a_d \quad (62)$$

where  $a_d$  is the Stokes-Einstein radius of the macromolecular drug. Once  $k_{\text{coal}}$  is determined, eq 61 can be used with  $\bar{R} = a_d$  to determine the induction time, namely,

$$t^d = \frac{4r_0^2 [\epsilon_M(0) + \epsilon_\mu(0)] a_d}{R_M(0)^3 k_{\text{coal}}} \quad (63)$$

Although the particle radius  $r_0$  appears explicitly in the forementioned expression, the coalescence rate,  $k_{\text{coal}}$ , depends explicitly on the radius  $r_0$  at which it is measured. Specifically,  $k_{\text{coal}}$  increases proportionally with the microsphere surface area, meaning that the rate of pore growth per unit surface area (i.e.,  $k_{\text{coal}}/4\pi r_0^2$ ) is conserved.

**Continuous Release**—Following the induction time ( $> t^d$ ) Fickian diffusion of the drug through the porated microsphere allows the mass of drug remaining in the microparticle to be determined as follows<sup>24</sup>:

$$\begin{aligned} \frac{m_d(t)}{m_d(0)} &= 1 - \phi_d^{\text{burst}}(1 - e^{-k_d t}) - \\ &\quad (1 - \phi_d^{\text{burst}}) \left( 1 - \frac{6}{\pi^2} \sum_{j=1}^{\infty} \frac{e^{-j^2 \pi^2 \bar{D}_d^* (t-t^d)/r_0^2}}{j^2} \right) \quad (64) \end{aligned}$$

Note that eq 64 applies for all time because  $\bar{D}_d^* = 0$  for times  $t \leq t^d$ .

**Summary of Model**—In the preceding sections, an explicit quantitative model has been outlined for the prediction of mass loss, molecular weight change, and macromolecular drug release as functions of time for the case of a bulk-eroding

**Table 2—Input Variables for 50:50 PLGA/MN rgp 120 Microspheres**

| (a) Variable            | Description                           | Value  |
|-------------------------|---------------------------------------|--|
| $r_0$                   | radius of microsphere                 | 20 $\mu\text{m}$                                   |
| $M_{LA}, M_{GA}$        | monomer molecular weights             | 90.08, 76.05 $\text{g mol}^{-1}$                   |
| $\epsilon_{\mu}(0)$     | initial microporosity                 | 0.217  |
| $\epsilon_M(0)$         | initial mesoporosity                  | 0.096  |
| $\phi_0$                | occlusion porosity                    | 0.173  |
| $R_M(0)$                | initial mesopore radius               | 1.0 $\mu\text{m}$                                  |
| $N$                     | number of soluble oligomers           | 6  |
| $a_d$                   | drug radius                           | 62 $\text{\AA}$                                    |
| $M_d$                   | drug molecular weight                 | 104000 $\text{g mol}^{-1}$                         |
| $m_d(0)$                | initial mass of drug in a microsphere | 0.220 $\text{ng}$                                  |
| (b) Variable            | Description                           | Value  |
| $k_n$                   | random scission rate                  | $2.9 \times 10^{-4} \text{ day}^{-1}$              |
| $k_n^1$                 | end scission rate                     | $3.3 \text{ day}^{-1}$                             |
| $k_{\text{coal}}$       | rate of mesopore formation            | $0.36 \text{ day}^{-1}$                            |
| $t^d$                   | induction phase time                  | 8.6 days   |
| $\phi_d^{\text{burst}}$ | drug burst fraction                   | 0.2  |
| $k_d$                   | drug desorption constant              | $2.40 \text{ day}^{-1}$                            |
| $C_d^s(0)$              | drug adsorption concentration         | $4.22 \times 10^{-12} \text{ mol cm}^{-2}$         |
| $\bar{D}_d^s$           | effective drug diffusivity            | $2.00 \times 10^{-13} \text{ cm}^2 \text{ s}^{-1}$ |

microsphere containing a macromolecular drug. The main assumptions of the analysis have been outlined at the outset. Among the “working” equations, we note here the following:

(1) The amount of oligomer  $n_i(t)$  of length  $i$  can be determined either analytically by eqs 38–40 or numerically by eqs 41–45 for the cases of random chain scission, end scission, or a combination of both.

(2) The mass and mean molecular weights of the microsphere (including the weight fraction distribution) can be determined from Table 1.

(3) An initial burst of macromolecular drug release is predicted on the basis of eq 52 (or in combination with degradation-controlled-release by eq 64).

(4) Following an “induction” time, predicted by eq 63, drug is released in a manner as predicted by eq 64.

Actual implementation of these equations for the prediction of microsphere erosion and macromolecular drug release behavior requires knowledge of a number of geometrical, kinetic, and physicochemical transport parameters for the specific system under study. Although many of these can be easily measured, some require further modeling efforts. In the next section we demonstrate how experimental data may be used with the model as it stands to estimate unknown transport parameters appearing in the model and use of the model to provide detailed predictions of erosion and macromolecular drug release from PLGA microspheres.

### Paradigm for Specific Calculations

The model outlined in this article can serve the need for a predictive theory of macromolecule release from bulk-eroding microspheres, especially given specification of the physicochemical parameters for a particular system. These parameters are listed in Table 2. The specific values listed are appropriate to the protein-loaded PLGA microspheres studied elsewhere<sup>8</sup> and examined using this model in the following discussion. The first tier of values (labeled a) denote values that are readily obtained by direct experimental observation. The second tier of values (labeled b) must be determined indirectly by careful examination of the erosion and release behavior of the microsphere in a given set of conditions, as subsequently described.

Once the values listed in Table 2 have been determined, the model can be used to explore microsphere controlled-release performance in a variety of conditions. For example, it is possible to change the geometrical configuration of the microparticle system, by varying the sphere radius ( $r_0$ ) or even by changing the particle shape. A merit of this model is that the performance of the new microparticle entity can immediately be predicted; that is, the model can be used to “design” microparticle controlled-release systems to meet therapeutic aims, without necessarily designing and testing all the various possible alternative systems.

In the remainder of this section, a paradigm is developed on the basis of the preceding model for interpretation of bulk polymer erosion and protein release data, to which attention is directed in the next section. A few simplifications have been made to permit an easily tractable paradigm. First, we assume the initial micropore and mesopore distributions to be uniform [radii  $R_{\mu}(0), R_M(0)$ ]. No assumptions have been made regarding the initial polymer molecular weight distribution nor the size or number of drug occlusions. Also, it is assumed that only oligomers of chain length 1 to  $N$  are released as degradation products. Finally, it is useful to consider specifically the case of PLGA microspheres, with drug initially localized in the macropores (occlusions) of the polymer particle (i.e., as in Figure 1). In this case, for instance, the hydrophilic nature of the drug will manifest itself in terms of an induction time  $t^d > 0$ . If this were a hydrophobic drug, then Fickian release would occur immediately  $t^d = 0$  in unison with desorption.

Next, a paradigm is outlined for the case of PLGA microspheres containing a macromolecular drug on the basis of which the various constants appearing in the preceding equations can be determined:

(1) Measure the initial properties given in Table 2 (a) and the initial weight fraction of polymer of chain length  $i$ ,  $w_i(0)$ .

(2) Determine the random scission rate  $k_n$  and the end scission rate  $k_n^1$  by matching (for example) the “mass half-time”,  $t_{1/2}^m$ , of the measured particle mass fraction

$$\frac{m_p^{\text{part}}(t_{1/2}^m)}{m_p(0)} \stackrel{\text{def}}{=} \frac{1}{2} \quad (65)$$

and the “molecular weight half-time”,  $t_{1/2}^w$ , of the measured weight averaged mean molecular weight

$$\frac{\bar{M}_w^{\text{part}}(t_{1/2}^w)}{\bar{M}_w^{\text{part}}(0)} \stackrel{\text{def}}{=} \frac{1}{2} \quad (66)$$

Because the profile of  $\bar{M}_n(t)$  is not used in evaluating  $k_n$  and  $k_n^1$ , its prediction can be compared with the experimental measurements as a *test of the analysis*. The values determined for  $k_n$  and  $k_n^1$  can give insight into the degradation mechanisms of the proposed model.

(3) Measure the rate of mesopore formation at the surface of the microparticles by visual observation at various times of degradation and deduce  $k_{\text{coal}}$ .<sup>25</sup>

(4) Predict the time of the induction phase  $t^d$ , given  $R_M(0)$ , using eq 63. Compare this value with the experimental observed value as a *test of the analysis*.

(5) Measure the fraction of drug released during the initial burst phase and the initial slope of the burst (or perhaps the time required for 95% of the burst to be complete) and use eqs 52 and 53 to calculate both the rate constant of desorption  $k_d$  and the surface concentration of adsorbed drug  $C_d^s(0)$ .

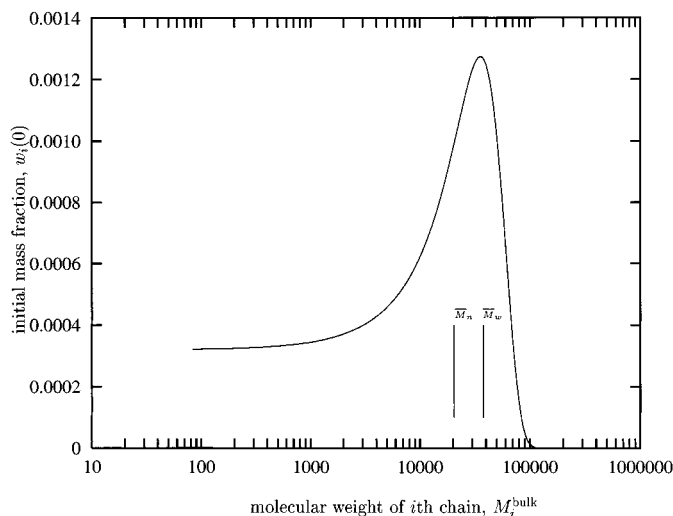


**Figure 3**—Initial molecular weight distribution for 50:50 PLGA polymer microspheres considered here. The initial mass- and number-averaged mean molecular weights are also shown.

(6) Measure the half-time of the drug mass released following the induction phase and deduce, via eq 64 and an iterative procedure,  $D_d^*$ .

(7) All of the necessary constants are now known. Predict  $m_p^{\text{part}}(t)$ ,  $m_d(t)$ ,  $\bar{M}_w^{\text{part}}(t)$ , and  $\bar{M}_n^{\text{part}}(t)$  and compare with the experimental data. Depending on the agreement between experimental data and theoretically predicted curves, as well as the absolute values of rate constants [ $k_n$ ,  $k_p^1$ ,  $k_{\text{coal}}$ ], the diffusion-controlled or degradation-controlled nature of the erosion/release process can be analyzed, as well as the suitability of the model.

The strategy just outlined for characterizing the erosion and release behavior of bulk-eroding microspheres involves determination of various microparticle features (see, e.g., step 3) that may not have been explicitly determined in many published experimental studies concerned with microparticle erosion and/or macromolecular drug release. The comparisons made in the next section are therefore primarily devoted to a consideration of a companion experimental study involving protein release from PLGA particles.<sup>8</sup>

### Comparison with Experimental Data

In this section, we illustrate the use of the paradigm just outlined to deduce the transport and degradation rate constants describing the degradation of 50:50 PLGA microspheres and simultaneous release of the model protein gp120. We also give brief consideration to protein release data appearing in the literature that do not display the signature burst-delay-burst behavior exhibited by the gp120 system.

**Application of the Paradigm**—Following step 1 of the paradigm, Table 2 (a) provides a list of pertinent physical and geometrical parameters characterizing the microspheres. The initial polymer distribution of these experiments<sup>8</sup> is shown in Figure 3. This initial distribution is characterized by  $\bar{M}_w(0) = 37954 \text{ g mol}^{-1}$  and  $\bar{M}_n(0) = 20462 \text{ g mol}^{-1}$ . The “apparent” molecular weight of a characteristic monomer is  $M_1^{\text{bulk}} = 83 \text{ g mol}^{-1}$ , and the molecular weight of the  $i$ th chain is given by eq 9.

Microsphere mass, and mass- and number-averaged mean molecular weights as functions of time for various models of the degradation process are displayed in Figures 4, 5, and 6.

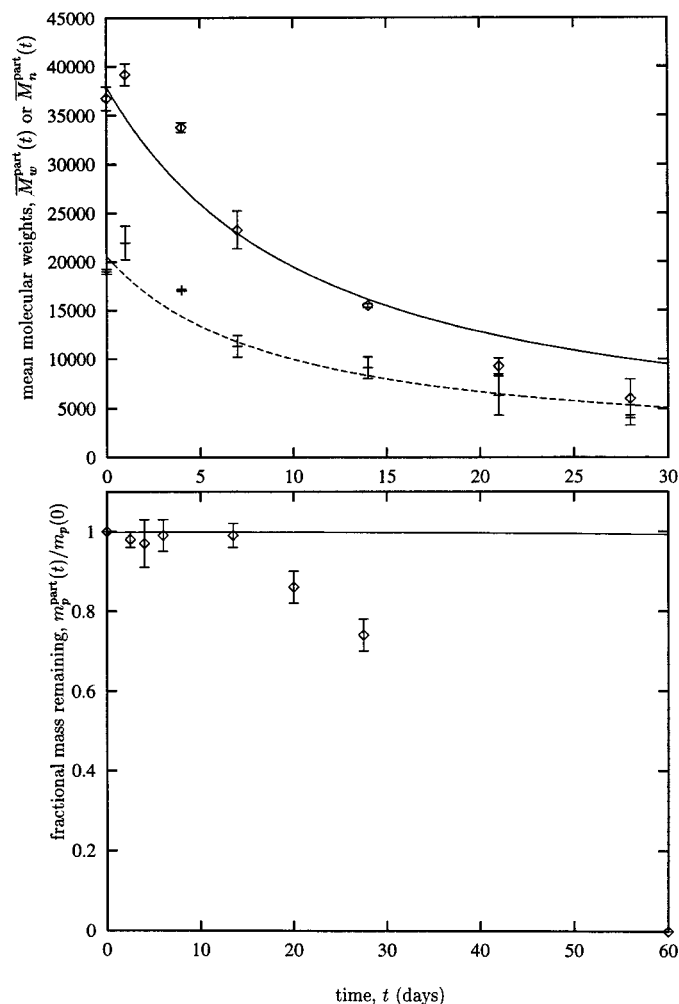


**Figure 4**—Microparticle transient data as a function of time. Theoretical predictions from the random scission model (lines) are compared with experimental data (points).

The experimental data suggests that the relevant half-times are

$$t_{1/2}^m = 35 \text{ days} \quad (67)$$

$$t_{1/2}^w = 10.5 \text{ days} \quad (68)$$

Figure 4 assumes the degradation process occurs only by random chain scission. The correct prediction of  $t_{1/2}^w$  with this model is obtained by  $k_n^1 = k_n = 3.6 \times 10^{-4} \text{ days}^{-1}$ . An important result here is that, whereas the molecular weight prediction is correct if one assumes random scission kinetics, the mass prediction is clearly invalid. This result suggests that random chain scission cannot account for the experimentally observed behavior of PLGA degradation. The reason underlying the poor fit of mass loss is that too few low molecular weight (i.e., soluble and diffusing) oligomers are formed to account for the observed mass loss. The other extreme, that of an end scission model is shown in Figure 5. The correct prediction of  $t_{1/2}^w$  with this model is obtained with  $k_n^1 = 23 \text{ day}^{-1}$ , and  $k_n = 0$ . In this case, unlike that of random chain scission, too much mass loss is predicted relative to what is observed (i.e., too many small oligomers are formed). This result suggests that the actual degradation mechanism involved in PLGA hydrolytic degradation consists of both random scission and end scission. Mechanistically, this can

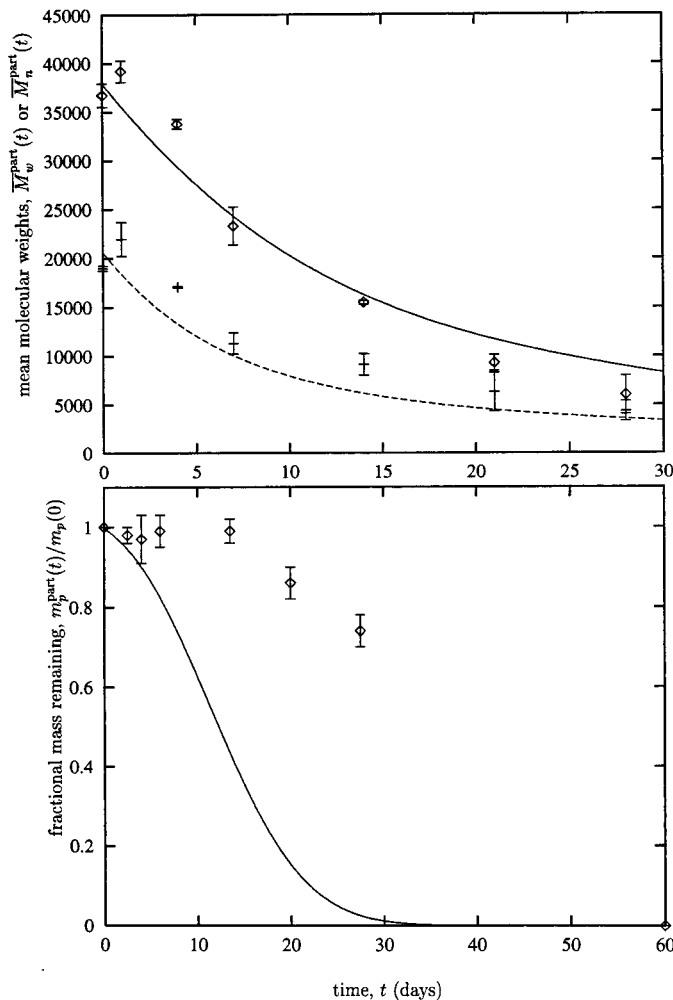


**Figure 5**—Microparticle transient data as a function of time. Theoretical predictions from the *end scission* model (lines) are compared with experimental data (points).

be explained by the increase in acidity of the end groups, and, hence, the relatively large rate constant near chain ends (see eqs 69 and 70). The result obtained by this combined model is shown in Figure 6. The correct predictions of  $t_{1/2}^w$  and  $t_{1/2}^m$  with this model are obtained with the following:

$$k_n^1 = 3.3 \text{ day}^{-1} \quad (69)$$

$$k_n = 2.9 \times 10^{-4} \text{ day}^{-1} \quad (70)$$

In other words, a very good fit of particle mass loss, number-averaged, and weight-averaged molecular weights can *only* be obtained by assuming *both* end and random chain scission, with the rate constants just given.

Visual observation of mesoscopic surface pores ( $R_M^d \approx 1 \mu\text{m}$ ; step 3 of the paradigm) shows that the rate of pore coalescence is linear in time,<sup>8</sup> with a rate of mesopore formation of  $k_{\text{coal}} = 0.36 \text{ day}^{-1}$ .

The mass release of protein as a function of time in PBS buffer is shown in Figure 7. The induction phase time is  $t^d \approx 8$  days. Given the value of  $k_{\text{coal}}$  already reported, using  $R_M(0) = 1.0 \mu\text{m}$ , and following step 4, we obtain from eq 63  $t^d = 8.6$  days, which is in fair agreement with the experimental observation.

Approximately 1/5 of the initial mass of drug contained in the microparticle is released during the burst phase ( $\phi_d^{\text{burst}} = 0.2$ ). Of this amount, 91% occurs in the first day. As described

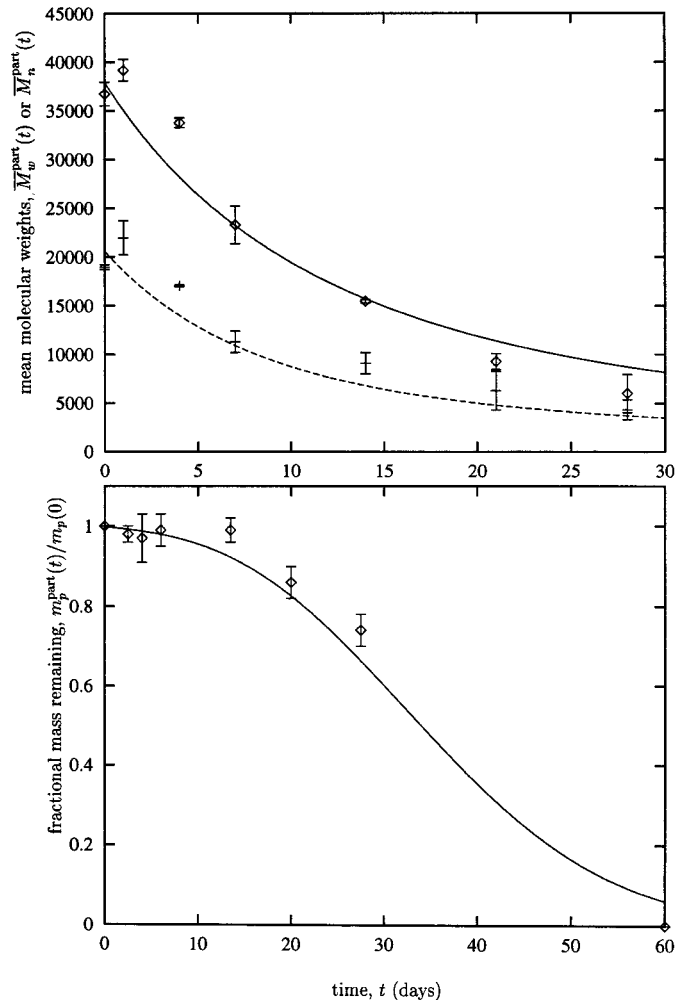


**Figure 6**—Microparticle transient data as a function of time. Theoretical predictions from the *combined scission* model (lines) are compared with experimental data (points).

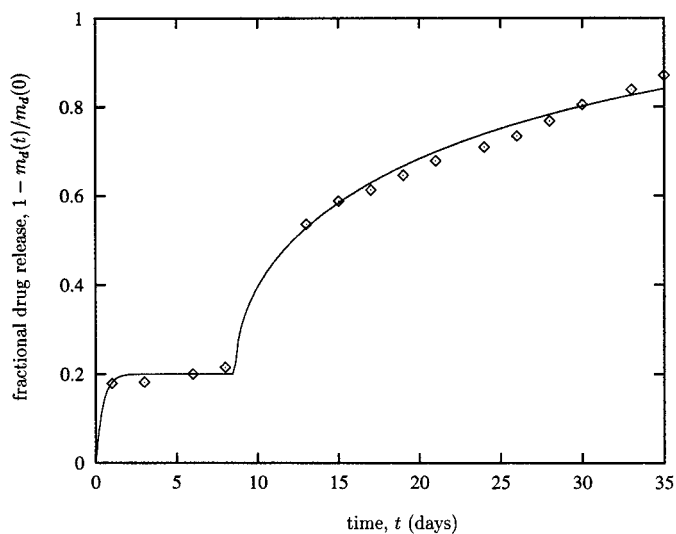


**Figure 7**—Fractional release of MN rpg 120 as a function of time. Theoretical prediction for  $t^d = 8.6$  days (solid line) is compared with experimental data (diamonds).

in step 5 of the paradigm, from eqs 52, and 53, and the value of  $R_M(0)$  just computed, this corresponds to a desorption constant of  $k_d = 2.40 \text{ day}^{-1}$ , and a surface concentration of

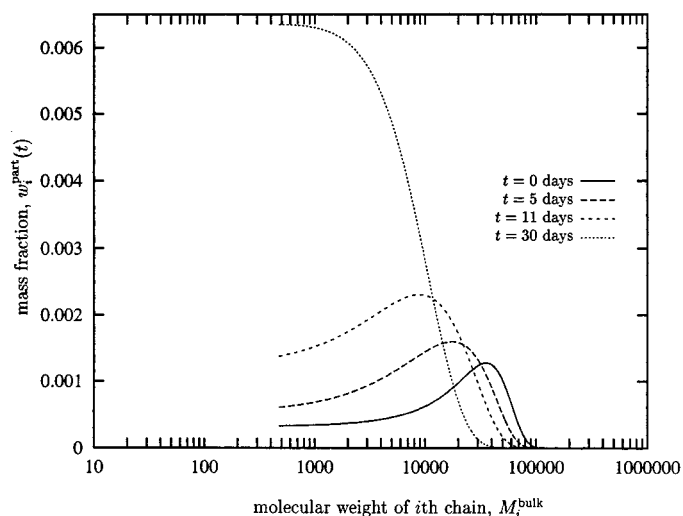


**Figure 8**—Microparticle molecular weight distribution during the hydration and erosion process. Shown are the distributions at 0, 5, 11, and 30 days (mid-erosion).

$C_d^s(0) = 4.22 \times 10^{-12}$  mol cm<sup>-2</sup>. This surface concentration corresponds to 19 μg/mg (adsorbed gp120 per mass of microsphere), a value that, strikingly, falls between the limits (5.1 and 24 μg/mg) reported for salmon calcitonin adsorption to PLGA microspheres for monolayer and multilayer adsorption.<sup>26</sup>

Finally, following step 6 of the paradigm, we have, from eq 64,  $\bar{D}_d^s = 2.00 \times 10^{-13}$  cm<sup>2</sup> s<sup>-1</sup>, a value that is again reasonable for large molecules diffusing through porous polymer matrices.<sup>27</sup>

All of the requisite transport data have now been gathered with the paradigm; hence, it is possible, as in step 7, to compare predictions of  $m_p(t)$ ,  $\bar{M}_w(t)$ ,  $\bar{M}_n(t)$ , and  $m_d(t)$  with experimental values. A comparison of mass-averaged and number-averaged mean molecular weights with the theoretical predictions is given in Figure 6a. The very good agreement between theory and experiment appears to strongly affirm the combined random scission and end scission, first-order degradation rate model underlying our theory. The actual polymer distributions are shown in Figure 8. The comparison of theory with experimental data for polymer mass loss is shown in Figure 6b. The initial insensitivity of mass with time in buffer is because random chain scission creates many large, insoluble oligomers and sufficient time has not elapsed for end scission to have accumulated soluble monomer units, which diffuse out of the polymer, leading to observed mass loss.

Finally, a comparison of experimental data and theoretical protein release predictions is shown in Figure 7. The reasonable agreement between the theory and experiment lends further support to the drug release model. Moreover, the closely related values of hydration and protein release induction times confirm results published elsewhere<sup>5</sup> for bovine serum albumin (BSA) release from PLGA slabs.

Particle mass (Figure 6b), molecular weight (Figure 6a) and protein release (Figure 7) predictions all reasonably match the experimental data. Also, the values deduced for various physical parameters (e.g., matrix hydration) and transport coefficients (e.g., diffusion coefficients) are near to expectations based on the results of independent studies. Given this general agreement, we next inquire on the physical interpretation of the degradation rate constants already determined; namely,

$$k_n^1 = 3.8 \times 10^{-5} \text{ s}^{-1} \quad (71)$$

$$k_n = 3.4 \times 10^{-9} \text{ s}^{-1} \quad (72)$$

These values represent the apparent rate constants of polymer scission by hydrolysis. The very large disparity between the magnitudes of these rate constants (in part, a reflection of the inherent rate differences between end- and midchain scission<sup>28</sup>) may reflect a concealed mass-transfer rate-limiting step in the random-scission hydrolysis of the polymer chains. Specifically, it is possible that the (generally insoluble) oligomers produced by scission along the length of the polymer chains act to transiently shield neighboring oligomers from water that has diffused into the polymer matrix, leading to an apparent reduction in the rate of random scission ( $k_n$ ). By contrast, end scission necessarily produces monomers that can immediately solubilize in surrounding water; hence, the 'extinction' process that potentially hinders the rate of random scission along the polymer chain does not hinder the end scission rate ( $k_n^1$ ), tending to magnify the disparity ( $k_n^1 > k_n$ ). A further potential source of disparity between the magnitudes of  $k_n^1$  and  $k_n$  is the initial molecular structure of the microparticle. It is conceivable that the ends of polymer chains have a greater probability of residing at a micropore surface than do chain interiors;<sup>29</sup> hence, hydrolysis will act more predominantly at the ends, manifested again by  $k_n^1 > k_n$ .

In any case, it appears important to note that very similar degradation rate constants are obtained by application of the model to other 50:50 PLGA degradation data appearing in the literature.<sup>30</sup> In the experimental study of Hausberger *et al.*,<sup>30</sup> microparticles possessed initial mean molecular weights of  $\bar{M}_w(0) = 36\,900$  and  $\bar{M}_n(0) = 25\,300$ , in one case (Case I), and  $\bar{M}_w(0) = 26\,100$  and  $\bar{M}_n(0) = 11\,300$  in a second case (Case II). We assumed initial oligomer distributions to be Gaussian in both cases. Very good matches of the predicted and experimental mass and mean weight- and number-averaged molecular weight kinetic profiles were obtained upon choosing  $k_n = 1.8 \times 10^{-9} \text{ s}^{-1}$  and  $k_n^1 = 2.7 \times 10^{-5} \text{ s}^{-1}$  in Case I, and  $k_n = 4.8 \times 10^{-9} \text{ s}^{-1}$  and  $k_n^1 = 2.6 \times 10^{-5} \text{ s}^{-1}$  in Case II. In both cases, these values agree reasonably well with the ( $k_n, k_n^1$ ) values deduced in eqs 71 and 72.

**General PLGA Degradation Constants**—The methodology for determining the end and random scission rates from the half-times of the mass and molecular weights is generalized in Table 3 for the purposes of use by other researchers. Given  $t_{1/2}^w$  and  $t_{1/2}^m$  (reported in days), one can obtain theoretical estimates of  $k_n^1$  and  $k_n$  directly from the Table 3. It should be noted that this table has been compiled with the initial distribution shown in Figure 3 [i.e., with  $\bar{M}_w(0) = 37\,954 \text{ g mol}^{-1}$  and  $\bar{M}_n(0) = 20\,462 \text{ g mol}^{-1}$  for a 50:50 PLGA system]. Thus, the application of Table 3 is restricted to these conditions, although similar tables could be easily prepared given alternative initial polymer data.

**Other Protein Release Profiles**—In the case just considered, we have assumed that the hydrophilic macromolecular drug is entirely contained within the macropores, or occlusions, of the microparticle. This assumption has led to the phenomenon of an "induction phase" prior to commencement of the Fickian drug release process, which lasts a finite duration following polymer hydration until the mesopores are sufficiently numerous to permit the escape of the (bulky) protein molecules. There are, however, bulk-eroding polymeric systems that do *not* display a marked induction-phase phenomenon, possibly because of a variety of causes. For example, very small hydrophilic drugs may rapidly diffuse through micropores, leading to a substantial release during the hydration phase of the polymeric particle. In this event, the assumption of a drug induction period does not hold and the entire drug release is governed by eq 64. For macromolecular substances, a "slow" desorption or "fast" hydration may lead to simultaneous desorption and Fickian diffusion pro-

**Table 3—Values of the End Scission Rate ( $k_n^1$ ) and the Random Scission Rate ( $k_n$ ) Given Observed Values of the Mass Averaged Mean Molecular Weight Half-Time ( $t_{1/2}^w$ ) and the Particle Mass Half-Time ( $t_{1/2}^m$ )**

| $t_{1/2}^w$ | $t_{1/2}^m$        |                       |         |                       |         |                       |                       |                       |
|-------------|--------------------|-----------------------|---------|-----------------------|---------|-----------------------|-----------------------|-----------------------|
|             | 20                 |                       | 30      |                       | 40      |                       | 50                    |                       |
|             | $k_n^1$            | $k_n$                 | $k_n^1$ | $k_n$                 | $k_n^1$ | $k_n$                 | $k_n^1$               | $k_n$                 |
| 6           | 5.49               | $5.08 \times 10^{-4}$ | 2.50    | $5.66 \times 10^{-4}$ | 1.41    | $5.94 \times 10^{-4}$ | $9.09 \times 10^{-1}$ | $6.04 \times 10^{-4}$ |
| 7           | 6.33               | $4.06 \times 10^{-4}$ | 2.91    | $4.67 \times 10^{-4}$ | 1.64    | $5.01 \times 10^{-4}$ | 1.05                  | $5.18 \times 10^{-4}$ |
| 8           | 7.14               | $3.27 \times 10^{-4}$ | 3.30    | $3.93 \times 10^{-4}$ | 1.87    | $4.26 \times 10^{-4}$ | 1.20                  | $4.43 \times 10^{-4}$ |
| 9           | 7.97               | $2.63 \times 10^{-4}$ | 3.68    | $3.35 \times 10^{-4}$ | 2.10    | $3.69 \times 10^{-4}$ | 1.35                  | $3.88 \times 10^{-4}$ |
| 10          | 8.76               | $2.11 \times 10^{-4}$ | 4.03    | $2.92 \times 10^{-4}$ | 2.32    | $3.23 \times 10^{-4}$ | 1.50                  | $3.42 \times 10^{-4}$ |
| 11          | 9.30               | $1.78 \times 10^{-4}$ | 4.41    | $2.50 \times 10^{-4}$ | 2.54    | $2.85 \times 10^{-4}$ | 1.64                  | $3.04 \times 10^{-4}$ |
| 12          | $1.00 \times 10^1$ | $1.41 \times 10^{-4}$ | 4.76    | $2.18 \times 10^{-4}$ | 2.75    | $2.53 \times 10^{-4}$ | 1.78                  | $2.73 \times 10^{-4}$ |
| 13          | $1.08 \times 10^1$ | $1.08 \times 10^{-4}$ | 5.08    | $1.92 \times 10^{-4}$ | 2.96    | $2.27 \times 10^{-4}$ | 1.92                  | $2.47 \times 10^{-4}$ |
| 14          | $1.15 \times 10^1$ | $7.94 \times 10^{-5}$ | 5.42    | $1.68 \times 10^{-4}$ | 3.16    | $2.03 \times 10^{-4}$ | 2.06                  | $2.24 \times 10^{-4}$ |
| 15          | $1.22 \times 10^1$ | $5.42 \times 10^{-5}$ | 5.74    | $1.46 \times 10^{-4}$ | 3.33    | $1.85 \times 10^{-4}$ | 2.10                  | $2.03 \times 10^{-4}$ |
| 16          | $1.30 \times 10^1$ | $2.94 \times 10^{-5}$ | 6.09    | $1.26 \times 10^{-4}$ | 3.55    | $1.65 \times 10^{-4}$ | 2.31                  | $1.88 \times 10^{-4}$ |
| 17          | $1.37 \times 10^1$ | $7.30 \times 10^{-6}$ | 6.42    | $1.08 \times 10^{-4}$ | 3.74    | $1.49 \times 10^{-4}$ | 2.45                  | $1.71 \times 10^{-4}$ |
| 18          |                    |                       | 6.73    | $9.30 \times 10^{-5}$ | 3.94    | $1.34 \times 10^{-4}$ | 2.58                  | $1.57 \times 10^{-4}$ |
| 19          |                    |                       | 7.08    | $7.80 \times 10^{-5}$ | 4.13    | $1.21 \times 10^{-4}$ | 2.71                  | $1.44 \times 10^{-4}$ |
| 20          |                    |                       | 7.39    | $6.47 \times 10^{-5}$ | 4.33    | $1.09 \times 10^{-4}$ | 2.83                  | $1.33 \times 10^{-4}$ |
| 21          |                    |                       | 7.70    | $5.26 \times 10^{-5}$ | 4.51    | $9.79 \times 10^{-5}$ | 2.97                  | $1.21 \times 10^{-4}$ |
| 22          |                    |                       | 8.00    | $4.13 \times 10^{-5}$ | 4.70    | $8.73 \times 10^{-5}$ | 3.10                  | $1.12 \times 10^{-4}$ |
| 23          |                    |                       | 8.34    | $2.99 \times 10^{-5}$ | 4.89    | $7.79 \times 10^{-5}$ | 3.22                  | $1.03 \times 10^{-4}$ |
| 24          |                    |                       | 8.68    | $1.92 \times 10^{-5}$ | 5.07    | $6.92 \times 10^{-5}$ | 3.34                  | $9.47 \times 10^{-5}$ |
| 25          |                    |                       | 9.04    | $9.00 \times 10^{-6}$ | 5.25    | $6.11 \times 10^{-5}$ | 3.46                  | $8.69 \times 10^{-5}$ |

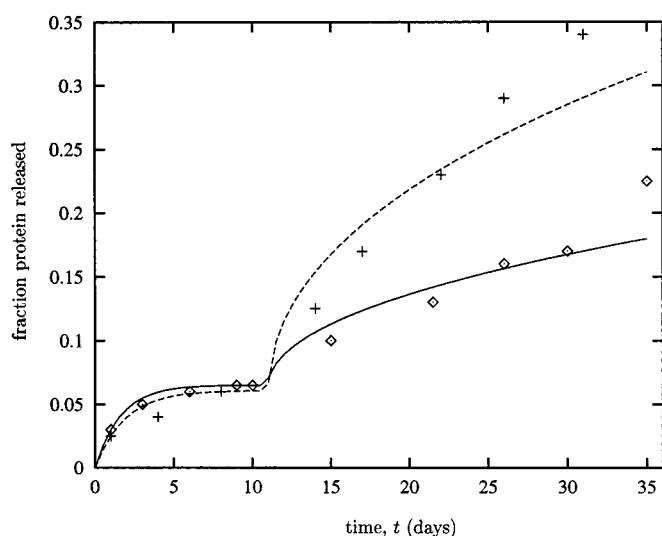


**Figure 9**—Experimental data of tetanus toxin release from PLA (diamonds) and PLGA (crosses) microspheres with weight average molecular weights of 100 000 Da. Both theoretical curves assume a drug induction time ( $t^*$ ) of 11 days. The theoretical curve for the PLA (solid line) is characterized by  $\phi_d^{\text{burst}} = 6.52 \times 10^{-2}$ ,  $k_d = 6.17 \times 10^{-1} \text{ day}^{-1}$ , and  $\bar{D}_d^* = 2.43 \times 10^{-14} \text{ cm}^2 \text{ s}^{-1}$ . On the other hand, the PLGA (dashed line) is characterized by  $\phi_d^{\text{burst}} = 6.09 \times 10^{-2}$ ,  $k_d = 5.28 \times 10^{-1} \text{ day}^{-1}$ , and  $\bar{D}_d^* = 1.25 \times 10^{-13} \text{ cm}^2 \text{ s}^{-1}$ . The radii of these high molecular weight microspheres were  $r_0 \approx 60 \pm 20 \mu\text{m}$  for both PLA and PLGA.

cesses, meaning that the “first” and “second” bursts are essentially indistinguishable.

As a purely illustrative example, we consider briefly a recent study<sup>7</sup> of the release of tetanus toxoid from PLA and 50:50 PLGA microspheres (Figures 9 and 10). In Figure 9, predictions are compared with the 100 KDa PLGA and PLA systems studied elsewhere,<sup>7</sup> whereas comparisons of the 3 KDa PLGA and PLA systems are summarized in Figure 10. Although the comparisons are merely illustrative (constants have not been systematically deduced as in the previous case considered), theory and experiment shows, particularly for the 3 KDa PLA system (Figure 10), that a marked second burst

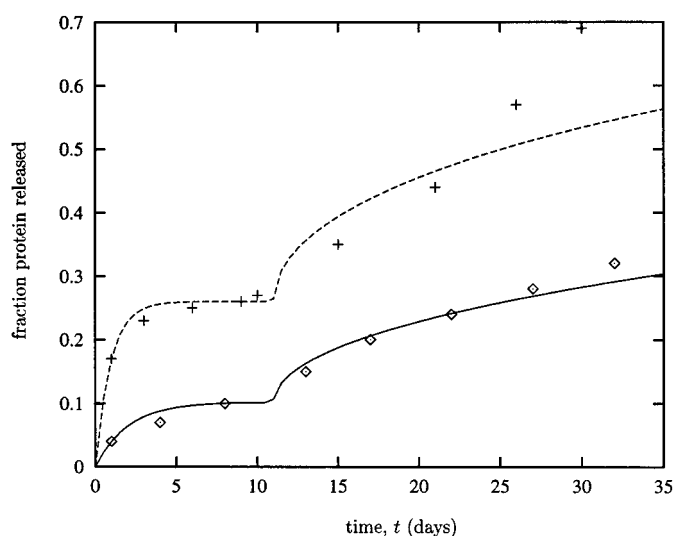


**Figure 10**—Experimental data of tetanus toxin release from PLA (diamonds) and PLGA (crosses) microspheres with weight average molecular weights of 3000 Da. Both theoretical curves assume a drug induction time ( $t^*$ ) of 11 days. The theoretical curve for the PLA (solid line) is characterized by  $\phi_d^{\text{burst}} = 1.02 \times 10^{-1}$ ,  $k_d = 4.99 \times 10^{-1} \text{ day}^{-1}$ , and  $\bar{D}_d^* = 1.95 \times 10^{-15} \text{ cm}^2 \text{ s}^{-1}$ . On the other hand, the PLGA (dashed line) is characterized by  $\phi_d^{\text{burst}} = 2.60 \times 10^{-1}$ ,  $k_d = 1.06 \text{ day}^{-1}$ , and  $\bar{D}_d^* = 3.30 \times 10^{-15} \text{ cm}^2 \text{ s}^{-1}$ . The radii of these low molecular weight microspheres were  $r_0 \approx 9 \pm 5 \mu\text{m}$  for PLA and  $r_0 \approx 6 \pm 3 \mu\text{m}$  for PLGA.

of protein release does not necessarily occur because of the (apparent) slow desorption and diffusion processes.

## Discussion

The model of macromolecule release from bulk-eroding microspheres outlined in this article may serve a variety of purposes. Indirectly, the model specifies geometrical and other physical parameters that should be known or measured if the transport parameters controlling erosion and release are to be determined by implementation of the paradigm. The

requisite "input" data are those listed in Table 2 (a), the values of which are either known from the literature or have been measured for a given system.<sup>8</sup> Knowing these parameters, by measurement of  $\bar{M}_w^{\text{part}}(t)$ ,  $m_p^{\text{part}}(t)$ , and  $m_d(t)$ , and by use of the paradigm, it is possible to determine: (i) the true polymer degradation rate constants for end scission ( $k_n^1$ ) and random scission ( $k_n$ ); (ii) the micropore coalescence rate constant ( $k_{\text{coal}}$ ); and (iii) the effective diffusivity ( $\bar{D}_d^*$ ) of the macromolecule through the eroding polymeric particle.

Having determined values for these parameters, allowing determination of the constants in Table 2 (b), predictions of weight- and number-averaged mean molecular weights ( $\bar{M}_w^{\text{part}}$ ,  $\bar{M}_n^{\text{part}}$ ), polymer mass ( $m_p^{\text{part}}$ ), and drug mass ( $m_d$ ) versus time can be made and compared with experimental data. It is essential to note that these deduced transport parameters are functions of copolymer composition, particle preparation method, and macromolecular drug type, yet *not* functions of particle size or shape or particle environment. That is, once the controlling transport parameters for a given microparticle system have been determined, predictions of erosion and release behavior in a variety of in vitro or in vivo environments, or for varying microparticle shapes and sizes, can be made. In addition, then, to the physical understanding that accompanies knowledge of the transport parameters ( $k_n$ ,  $k_n^1$ ,  $\bar{D}_d^*$ ; i.e., is the erosion process diffusion- or degradation-rate controlled?), a fully predictive theory is provided by knowledge of these same parameters. This theory can be used to predict particle performance in complex in vivo environments or particle shapes and sizes unlike those that have been used to determine the parameters by comparison with experimental data using the paradigm.

There are, however, certain limitations of the model as outlined here that ideally should be removed in the future. For the purpose of arriving at a tractable theory, only two rate-controlling pore populations have been assumed. In reality,<sup>8</sup> the micro- and mesopore distributions are not tightly localized about mean radii ( $R_\mu$ ,  $R_M$ ). In principle, broad distributions of pore radii can be included in a generalized model. However, in the present comparisons with experimental data, this limitation (chiefly impacting on the form of eq 63) for the prediction of  $t^d$  does not appear very restrictive.

Other limitations of the present model, which seem not to have adversely influenced the success of the present comparison with experimental data but may be restrictive for other systems, include the following: interactions between monomers (or oligomers) and pore walls have not been accounted for, nor have the effects of variable pH as necessarily accompanies solubilization of the acidic monomers of a bulk-eroding copolymer like PLGA in the microporous interstices of the polymer matrix. The effect of pH on the scission rate constants ( $k_n^1$  and  $k_n$ ) can, if necessary, be taken into account in the context of the present model. Perhaps most critical is the interaction between the encapsulated macromolecular drug and the polymer pore walls, although polymer swelling can also play a major role. Adsorption of protein to pore walls, protein configuration changes caused by polymer interactions or low pH, and protein-protein interactions can all be accounted for, as many macromolecular drugs possess the potential to display nonspecific interactions with the polymeric particle (or protein-protein interactions).<sup>26</sup>

Finally, it is highly desirable that formulation variables be related to the transport properties ( $k_n^1$ ,  $k_n$ ,  $\bar{D}_d^*$ ), so that the latter need not be deduced from particle performance studies, but might be estimated by choice of copolymer, preparation method, etc. One step in this direction might be to describe the drug diffusivity ( $\bar{D}_d^*$ ) by macrotransport theory<sup>31</sup> or free volume,<sup>32</sup> predictive methods that are highly developed for polymer diffusion processes and that permit establishment

of a relation between polymer environment and the physico-chemical nature of the diffusing substance.

## Glossary

|                           |  |
|---------------------------|--|
| $A$                       | area of particle involved in the desorption process  |
| $a_d$                     | drug radius (Stokes-Einstein radius)   |
| $a_i$                     | monomer radius (Stokes-Einstein radius)  |
| $B_{j,l}$                 | coefficients for combined model  |
| $C_d^s$                   | surface concentration of drug  |
| $\bar{D}^*$               | effective diffusivity  |
| $\bar{D}_d^*$             | effective drug diffusivity   |
| $\bar{D}_i^*$             | effective monomer diffusivity  |
| $F_{i,j}$                 | intrinsic rate that an ( $i + j$ )-mer breaks up into an $i$ -mer and a $j$ -mer                             |
| $J$                       | number of different types monomer subunits   |
| $j_i$                     | stoichiometric ratio coefficient of monomer type $i$   |
| $k_{\text{coal}}$         | pore coalescence rate constant   |
| $k_d$                     | drug desorption rate constant  |
| $k_n$                     | random scission rate constant  |
| $k_n^1$                   | end scission rate constant   |
| $M$                       | maximum chain length in the polymer  |
| $M_d$                     | molecular weight of drug   |
| $M_i$                     | molecular weight of monomer type $i$   |
| $\bar{M}_n$               | number-averaged mean molecular weight  |
| $\bar{M}_n^{\text{part}}$ | measured number-averaged mean molecular weight   |
| $\bar{M}_w$               | mass-averaged mean molecular weight  |
| $\bar{M}_w^{\text{part}}$ | measured mass-averaged mean molecular weight   |
| $M_{\text{GA}}$           | molecular weight of glycolic acid  |
| $M_{\text{H}_2\text{O}}$  | molecular weight of water  |
| $M_{\text{LA}}$           | molecular weight of lactic acid  |
| $M_i^{\text{bulk}}$       | apparent molecular weight of monomers  |
| $M_i^{\text{bulk}}$       | apparent molecular weight of oligomers of length $i$   |
| $m_d$                     | mass of drug present in microsphere  |
| $m_p$                     | total mass of polymer comprising microsphere   |
| $m_p^{\text{part}}$       | actual (measured) mass of polymer comprising microsphere—ignores the first $N$ oligomers in the distribution |
| $N$                       | number of soluble oligomers (chain length 1 to $N$ )   |
| $N_M$                     | number of mesopores at a radius $r$ within the microparticle   |
| $N_\mu$                   | number of micropores at a radius $r$ within the microparticle  |
| $n_i$                     | number of moles of oligomer of length $i$ present in microsphere   |
| $n_i^r$                   | discretized form of $n_i$  |
| $P(l,x)$                  | incomplete gamma function  |
| $\text{Pe}_R$             | Peclet number based on pore radius   |
| $R$                       | pore radius  |
| $\bar{R}$                 | mean pore radius leading from macropores to the external bath  |
| $R_M$                     | mesopore radius  |
| $R_\mu$                   | micropore radius   |
| $r$                       | radial position in spherical coordinates   |
| $r_0$                     | initial microparticle radius   |
| $t$                       | time   |
| $t^d$                     | drug induction time  |
| $t_m^{1/2}$               | mass half-time   |
| $t_w^{1/2}$               | mass-averaged mean molecular weight half-time  |

|                         |  |
|-------------------------|--|
| $V_0$                   | volume of macropores   |
| $w_i$                   | mass fraction of $i$ th chain based on total polymer mass $m_p$                  |
| $w_i^{\text{part}}$     | mass fraction of $i$ th chain based on measured polymer mass $m_p^{\text{part}}$ |
| $\hat{w}_i$             | useful variant of $w_i$  |
| $\epsilon$              | microparticle porosity   |
| $\epsilon_M$            | porosity due to macropores   |
| $e_\mu$                 | porosity due to micropores   |
| $\gamma$                | ratio of random to end scission rate constants                                   |
| $\phi_0$                | volume fraction of macropores  |
| $\phi_i$                | mole fraction of monomer $i$   |
| $\phi_d^{\text{burst}}$ | mass fraction of drug involved in the initial burst                              |
| $t$                     | dimensionless time based on $k_n^1$  |
| $\Delta\tau$            | discrete time step   |

## References and Notes

- Higuchi, T. Mechanism of sustained-action medication. Theoretical analysis of rate of release of solid drugs dispersed in solid matrices. *J. Pharm. Sci.* **1963**, *52*, 1145–1149.
- Lee, P. I. Diffusional release of a solute from a polymeric matrix—approximate analytical solutions. *J. Membr. Sci.* **1980**, *7*, 255–275.
- Joshi, A.; Himmelstein, K. J. Dynamics of controlled release from bioerodible matrices. *J. Controlled Release* **1991**, *15*, 95–104.
- Cleland, J.; Powell, M.; Lim, A.; Barron, L.; Berman, P.; Eastman, J.; Nunberg, T.; Wrin, X.; Vennari, J. Development of a single shot subunit vaccine for HIV-1. *AIDS Res. Human Retrovirus* **1994**, *10*, S21–S26.
- Shah, S. S.; Cha, Y.; Pitt, C. G. Poly(glycolic acid-co-DL-lactic acid): diffusion or degradation controlled drug delivery? *J. Controlled Release* **1992**, *18*, 261–270.
- Lewis, D. H. Controlled release of bioactive agents from lactide/glycolide polymers. In *Biodegradable Polymers as Drug Delivery Systems*; Chasin, X., Langer, X., Eds.; Marcel Dekker: New York, 1990; pp 1–41.
- Alonso, M. J.; Gupta, R. K.; Min, C.; Siber, G. R.; Langer, R. L. Biodegradable microspheres as controlled-release tetanus toxoid delivery systems. *Vaccine* **1993**, *11*, 1–8.
- Hanes, J.; Hildgen, P.; Edwards, D. A.; Battycky, R. P.; Coleman, S.; Cleland, J.; Langer, R. Poly(D,L-lactide-co-glycolic acid) microsphere degradation and pulsatile release of the globular protein gp 120. Submitted for publication in *J. Pharm. Sci.*
- Van Koevelen, D. W. *Properties of Polymers—Correlations with Chemical Structure*; Elsevier: Amsterdam, 1972.
- Cha, Y.; Pitt, C. G. A one-week subdermal delivery system for l-methadone based on biodegradable microcapsules. *J. Controlled Release* **1988**, *7*, 69–78.
- As pointed out in the discussion section, the general analysis outlined herein applies to far more general circumstances than those of microparticles into which water tunnels via straight, regularly shaped 'free molecular volume' cylindrical pores.
- Shih, C. Chain-end scission in acid catalyzed hydrolysis of poly(D,L-lactide) in solution. *J. Controlled Release* **1995**, *34*, 9–15.
- Shih, C.; Waldron, N.; Zentner, G. M. Quantitative analysis of ester linkages in poly(D,L-lactide) and poly(D,L-lactide-co-glycolide). *J. Controlled Release* **1996**, *38*, 69–73.

- Mark, H.; Simha, R. Degradation of long chain molecules. *Trans. Faraday Soc.* **1940**, *35*, 611–618.
- Montroll, E. W.; Simha, R. Theory of depolymerization of long chain molecules. *J. Chem. Phys.* **1940**, *8*, 721.
- Aris, R.; Gavalas, G. R. 1966 On the theory of reactions in continuous mixtures. *Phil. Trans. R. Soc. Lond.* **1966**, *A260*, 351–393.
- Ziff, R. M.; McGrady, E. D. The kinetics of cluster fragmentation and depolymerisation. *J. Phys. A: Math. Gen.* **1985**, *18*, 3027–3037.
- Ziff, R. M.; McGrady, E. D. Kinetics of polymer degradation. *Macromolecules* **1986**, *19*, 2513–2519.
- Kehlen, H.; Rätzsch, M. T.; Bergmann, J. Continuous kinetics of first order degradation reactions in polydisperse mixtures. *Chem. Eng. Sci.* **1988**, *43*, 609–616.
- Wang, M.; Smith, J. M.; McCoy, B. J. Continuous kinetics for thermal degradation of polymer in solution. *AIChE J.* **1995**, *41*, 1521–1533.
- Emsley, A. M.; Heywood, R. J. Computer modelling of the degradation of linear polymers. *Polymer Degradation Stability* **1995**, *49*, 145–149.
- Abramowitz, M.; Stegun, I. A. *Handbook of Mathematical Functions*. Dover: New York, 1965.
- In effect, eqs 41–44 are an explicit method for inverting a triangular matrix.
- Carslaw, H. S.; Jaeger, J. C. *Conduction of Heat in Solids*. Oxford, Oxford University 1959.
- This method of measurement is obviously approximate. Distinct mesopores become apparent by visual inspection of electron microscopic photos<sup>8</sup> when mesopores reach a radius of approximately  $R_M \approx 1 \mu\text{m}$ . Measuring the rate of growth of pores in the domain  $R_M \geq 1 \mu\text{m}$  may or may not be equivalent to measuring the rate constant  $k_{\text{coal}}$ .
- Calis, S.; Jeyanthi, R.; Tsai, T.; Mehta, R.; DeLuca, P. P. Adsorption of salmon calcitonin to PLGA microspheres. *Pharm. Res.* **1995**, *12*, 1072–1076.
- Saltzman, W. M.; Pasternak, S. H.; Langer, R. Microstructural models for diffusive transport in porous polymers. In *Controlled-Release Technology: Pharmaceutical Applications*; Lee, X., Good, X., Eds.; American Chemical Society: 1987; pp 16–33.
- Grandfils, C.; Flandroy, P.; Jérôme, R. Control of the biodegradation rate of poly(D,L-lactide) microparticles intended as chemoembolization materials. *J. Controlled Release* **1996**, *38*, 109–122.
- Gref, R.; Minamitake, Y.; Peracchia, M. T.; Trubetskoy, V.; Torchilin, V.; Langer, R. Biodegradable long-circulating polymeric nanospheres. *Science* **1994**, *263*, 1600.
- Hausberger, A. G.; Kenley, R. A.; DeLuca, P. P. Gamma Irradiation Effects on Molecular Weight and *in Vitro* Degradation of Poly(D,L-Lactide- CO-Glycolide) Microparticles. *Pharm. Res.* **1995**, *12*, 851–856.
- Brenner, H.; Edwards, D. A. *Macrotransport Processes*; Butterworth-Heinemann, Boston 1993.
- Duda, J. L.; Zielinski, J. M. 1996 Free-volume theory. In *Diffusion in Polymers*; Neogi, P., Ed.; Marcel Dekker: New York, 1996; pp 143–171.

## Acknowledgments

This work was supported partially by NIH grants GM26698 (RL) and HD29125 (RL and JH), as well as by Dow funds (RB and DAE). Special thanks are made to Blair Jackson and Cedomila Ristic for helpful technical advice.

JS9604117